Second-order Talbot self-imaging effect in the time domain

Hong-Guo Li, Rui-Xue Zhang, Zhan-Dong Liu, and Zong-Guo Li*
School of Science, Tianjin University of Technology, Tianjin 300384, China

(Received 28 January 2019; published 23 July 2019)

Different from classical Talbot self-imaging, second-order spatial Talbot effect is a kind of second-order imaging, in which the self-imaging of an object is observed through intensity correlation measurement. Here, in terms of space-time duality, we investigate the temporal counterpart of second-order Talbot self-imaging with temporally incoherent light. Our work shows that second-order Talbot effect in the time domain is related to the joint dispersion of light pulse in dispersive medium. Particularly, based on the discrete Fourier transformation, the fractional Talbot self-imaging via intensity correlation doesn't generally possess a definite fractional period, which contradicts some articles' results. Our results may be useful for implementing the repetition-rate-multiplication technique and remotely transmitting the periodic temporal signals robustly.

DOI: 10.1103/PhysRevA.100.013846

I. INTRODUCTION

The Talbot self-imaging effect as a kind of first-order imaging was first observed through the intensity distribution in 1836 by Henry Fox Talbot [1]. Lord Rayleigh later derived the formula of Talbot length and interpreted this effect as a consequence of Fresnel diffraction [2]. This phenomenon has been used in many applications including optical measurement [3], waveguide arrays [4], x-ray imaging [5], etc. Recently, many studies have shown that the second-order Talbot self-imaging effect in spatial domain can be performed either with entangled photon pairs [6–8] or with pseudothermal light [9–11]. The essential nature of the second-order Talbot self-imaging, different from classical Talbot effect, lies in the spatial correlation of entangled photons or thermal light fields. Hence, similar to ghost imaging, the second-order Talbot self-imaging effect also can be categorized to the second-order imaging.

By taking into account the duality between the paraxial diffraction of light beams in space and the temporal dispersion of narrow-band pulses in dispersive medium, the temporal analogies of many spatial systems were presented, such as ultrahigh-speed optical signal processing [12], ultrafast optical oscilloscope [13,14], temporal imaging [15], and temporal cloaking [16]. Recently, this duality has also been applied to explore the temporal analog of ghost imaging [17–27].

Motivated by the similarity between ghost imaging and second-order Talbot effect, in this paper, we investigate the temporal counterpart of second-order Talbot self-imaging with temporally incoherent light according to the space-time duality. The second-order Talbot effect in the time domain discussed here could be applied to remotely transmit the periodic signal and multiply the repetition rate of periodical signal without the need of the dispersion compensation or cancellation. The paper is organized as follows. In Sec. II, we discuss the wave equations describing the paraxial diffraction and dispersion, and then present the impulse response functions in the time domain for several typical optical systems. The analysis of the second-order Talbot effect in the time domain is presented in Sec. III. Finally, we make the conclusion in Sec. IV.

II. WAVE EQUATIONS AND IMPULSE RESPONSE FUNCTIONS IN THE TIME DOMAIN

We adopt the wave equations to describe paraxial diffraction and the narrow-band dispersion [28], respectively. Considering that the paraxial rays lie close to the optical axis z, i.e., the phase variation mostly exists along the axis z, we can express the optical field distribution as

$$\psi(x, y, z) = E(x, y, z)\exp(ikz), \tag{1}$$

where k is the wave number and $E(x, y, z)$ is a slowly varying envelope function relative to k. Due to the wave equation satisfying the Helmholtz equation

$$\nabla^2\psi + k^2\psi = 0, \tag{2}$$

when substituting Eq. (1) into the Helmholtz equation, we can obtain the reduced wave equation

$$\frac{\partial^2 E}{\partial x^2} + \frac{\partial^2 E}{\partial y^2} + \frac{\partial^2 E}{\partial z^2} + 2ik\frac{\partial E}{\partial z} = 0. \tag{3}$$

As $E(x, y, z)$ is a slowly varying envelope function, the paraxial approximation is usually taken into account,

$$\left|\frac{\partial^2 E}{\partial z^2}\right| << \left|2k\frac{\partial E}{\partial z}\right|. \tag{4}$$

Under this approximation, Eq. (3) becomes

$$\frac{\partial^2 E}{\partial x^2} + \frac{\partial^2 E}{\partial y^2} + 2ik\frac{\partial E}{\partial z} = 0. \tag{5}$$

Equation (5) is called the paraxial wave equation characterizing paraxial diffraction. For simplicity, we just consider the transverse one-dimensional case of the paraxial diffraction

*zgli@tjut.edu.cn

equation. One of its exact solutions is

$$E(x, y, z) = \iint E(x_0, y_0, 0)h(x, y; x_0, y_0)dx_0dy_0, \tag{6}$$

where $E(x_0, y_0, 0)$ and $E(x, y, z)$ are the optical field distributions at the initial position $(x_0, y_0, 0)$ and a final position (x, y, z), respectively, and $h(x, y; x_0, y_0)$ is the impulse response function in free space from the initial position to the final position (x, y, z). This impulse response function $h(x, y; x_0, y_0)$ is written as

$$h(x, y; x_0, y_0) = \frac{k}{i2\pi z}\exp\left\{\frac{ik}{2z}\left[(x - x_0)^2 + (y - y_0)^2\right]\right\}. \tag{7}$$

The above exact solution Eq. (6) can also be obtained according to Fresnel diffraction theory, which is called Fresnel diffraction integral [28,29]. This implies there is a link between the paraxial wave equation and Fresnel diffraction theory.

As for a differential equation that describes the temporal dispersion of narrow-band pulses propagating in a dispersive medium, we can utilize the similar approach as in the space domain. In terms of the first-order dispersion approximation [29], the differential equation in the time domain can be written as

$$\frac{\partial^2 E}{\partial \tau^2} + \frac{2i}{\beta}\frac{\partial E}{\partial l} = 0, \tag{8}$$

where β is the group velocity dispersion coefficient and E denotes the optical field distribution which is related to both the time τ and the distance l propagating in the dispersion medium like single-mode optical fiber. Obviously, Eq. (8) describing dispersion has the same form as the paraxial wave equation. Hence the dispersion can be regarded as the temporal analog of the paraxial diffraction, which is the duality between the paraxial diffraction and the dispersion. Therefore, the solution of Eq. (8) has the same mathematical form as that of the paraxial wave equation, which is

$$E(l, \tau) = \int E(0, \tau_0)h(\tau, \tau_0)d\tau_0, \tag{9}$$

where $h(\tau, \tau_0)$ is the temporal impulse response function characterizing the response at time τ to an input impulse at τ_0 in a dispersive medium. This impulse response function $h(\tau, \tau_0)$ can be expressed as

$$h(\tau, \tau_0) = \sqrt{\frac{1}{2\pi i\Phi}}\exp\left[\frac{i}{2\Phi}(\tau - \tau_0)^2\right], \tag{10}$$

where $\Phi = \beta l$ indicates the group delay dispersion (GDD) parameter of the dispersion medium. The GDD parameter can be manipulated by l, the length of dispersion medium like optical fiber.

Based on the duality between the paraxial diffraction and the dispersion discussed above, the temporal impulse functions of several typical optical systems can be obtained. Similar to the spatial object, the impulse response function of a temporal object can be expressed as

$$h(\tau, \tau_0) = P(\tau_0)\delta(\tau - \tau_0), \tag{11}$$

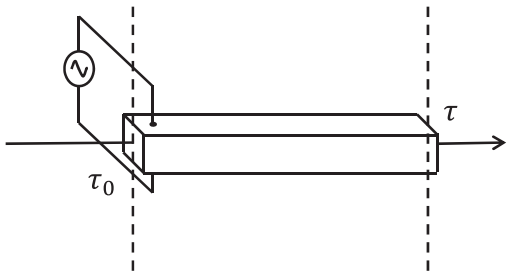

FIG. 1. Temporal lens is performed with an electro-optic modulator. The light pulse inputs at time τ_0 and outputs at time τ.

where $P(\tau)$ is a function describing the temporal structure of the temporal object.

For the temporal lens, it is used to imprint a quadratic phase modulation on the envelope of a light pulse. An ultrafast electro-optic modulator can act as a temporal lens, as shown in Fig. 1. Therefore, the impulse response function of the temporal lens can be expressed in the form

$$h(\tau, \tau_0) = \exp\left(-\frac{i\tau^2}{2\Phi_f}\right)\delta(\tau - \tau_0), \tag{12}$$

where Φ_f characterizes the focal time of the temporal lens.

Two sections of dispersion fiber and a temporal lens can form a temporal imaging system, as shown in Fig. 2. In terms of Eqs. (10) and (12), we can express the impulse response function of the temporal imaging system as

$$\begin{aligned} h(\tau, \tau_0) &= \int h(\tau', \tau_0)h(\tau'', \tau')h(\tau, \tau'')d\tau'd\tau'' \\ &= \frac{1}{2\pi i\sqrt{\Phi_2\Phi_1}}\exp\left(\frac{i\tau_0^2}{2\Phi_1} + \frac{i\tau^2}{2\Phi_2}\right) \\ &\quad\times\int\exp\left[\frac{i\tau'^2}{2}\left(-\frac{1}{\Phi_f} + \frac{1}{\Phi_1} + \frac{1}{\Phi_2}\right)\right. \\ &\quad\left. - i\tau'\left(\frac{\tau_0}{\Phi_1} + \frac{\tau}{\Phi_2}\right)\right]d\tau', \end{aligned} \tag{13}$$

where $\Phi_1 = \beta l_1$ and $\Phi_2 = \beta l_2$.

If the imaging condition $\frac{1}{\Phi_1} + \frac{1}{\Phi_2} = \frac{1}{\Phi_f}$ is satisfied, the term including τ'^2 in Eq. (13) will disappear. Thus Eq. (13)

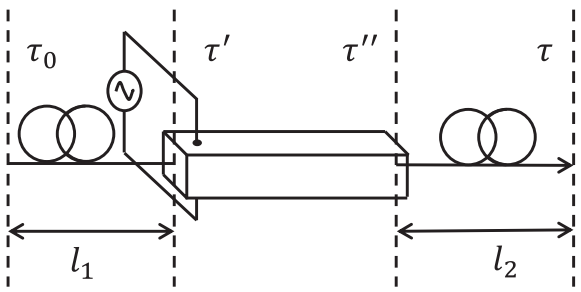

FIG. 2. Schematic view of a temporal imaging system. l_1 and l_2 denote the length of two optical fibers and τ represents the time.

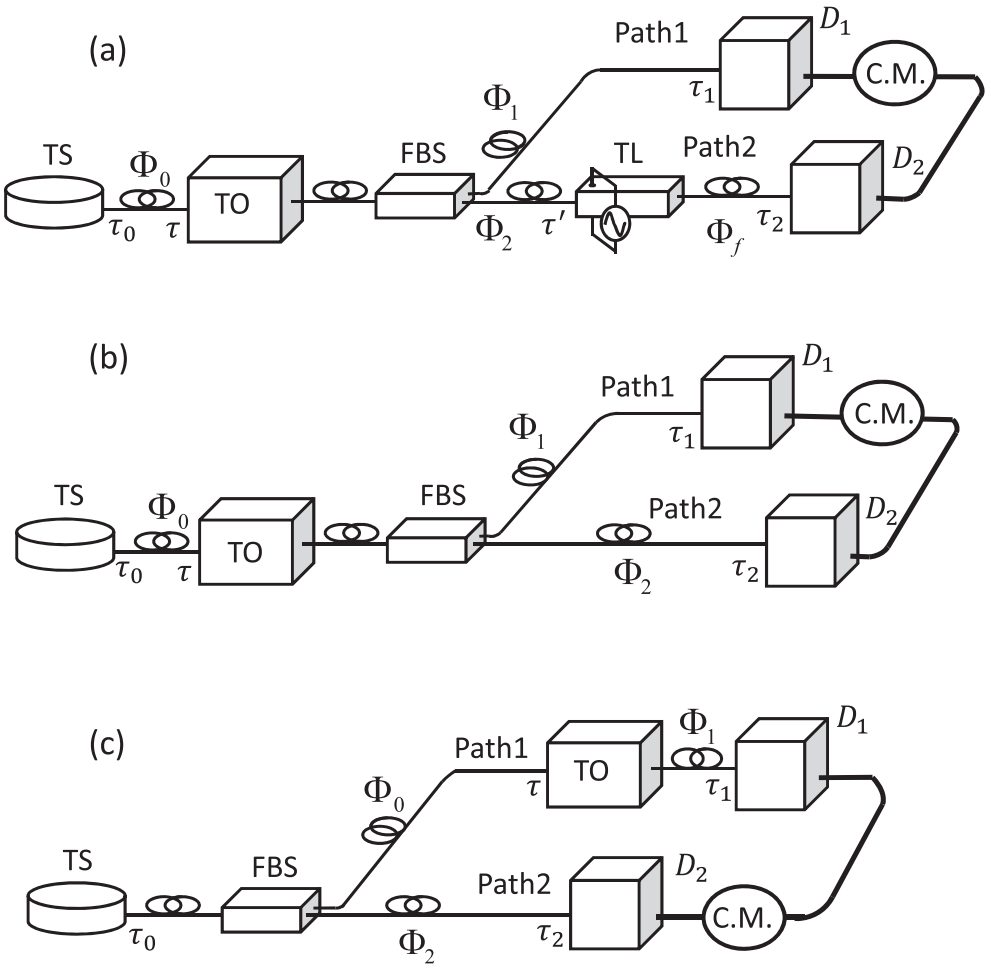

FIG. 3. Schematic illustration for second-order temporal Talbot self-imaging effect with temporally incoherent light. (a) Scheme I; (b) scheme II; (c) scheme III. TS denotes temporally incoherent light, TO is the temporal object, FBS is fiber beam splitter, TL is the temporal lens, two detectors D_1 and D_2 are used to detect the temporal signal, C.M. means intensity fluctuation correlation measurement, and τ denotes the time.

will be reduced to

$$h(\tau,\tau_0)=\frac{1}{i}\sqrt{\frac{\Phi_1}{\Phi_2}}\exp\left(\frac{i\tau_0^2}{2\Phi_1}+\frac{i\tau^2}{2\Phi_2}\right)\delta\left(\tau_0+\frac{\Phi_1\tau}{\Phi_2}\right). \quad (14)$$

If the imaging condition is not satisfied, Eq. (13) can be written as

$$h(\tau,\tau_0)=\frac{1}{\sqrt{2\pi i\Phi_R}}\exp\left\{\frac{i}{2\Phi_R}\left[\tau_0^2\left(1-\frac{\Phi_2}{\Phi_f}\right)+\tau^2\left(1-\frac{\Phi_1}{\Phi_f}\right)-2\tau\tau_0\right]\right\}, \quad (15)$$

where $\Phi_R=\Phi_1+\Phi_2-\frac{\Phi_1\Phi_2}{\Phi_f}$.

III. SECOND-ORDER TEMPORAL TALBOT SELF-IMAGING

In view of space-time duality, the temporal counterparts of second-order spatial Talbot self-imaging can be constructed as shown in Fig. 3, where three schemes are presented. Scheme I for second-order temporal Talbot self-imaging is illustrated in Fig. 3(a). We assume the source field $E_0(\tau_0)$ to be temporally complete incoherent

$$\langle E_0^*(\tau_0)E_0(\tau_0')\rangle=I_0\delta(\tau_0-\tau_0'), \quad (16)$$

where I_0 is a constant with the same dimension as the intensity. In practice, an amplified spontaneous emission source such as a broad-area superluminescent diode light source can be treated as a fully temporal incoherent light source approximately [30]. The pulse emitting from the source is coupled into a dispersive medium such as a section of single-mode optical fiber and then modulated by the temporal object. The pulsed light carrying the object information is then divided into two beams by the fiber beam splitter. In path 1, the pulse after propagating through a dispersive medium is received by the detector D_1, while path 2 consists of a temporal lens and the dispersive media. The detector D_2 is employed to measure the intensity of light at the end of path 2.

We now study the evolution of second-order temporal Talbot imaging, which is represented by the evolution of the intensity fluctuation correlation of the correlated pulsed light propagating through two dispersive media in scheme I. With the help of Eqs. (10)–(12), the impulse response functions

from the temporal incoherent light source to the detectors D_1 and D_2 are, respectively, written as

$$h_1(\tau_1,\tau_0)=\frac{1}{2\pi i\sqrt{\Phi_0\Phi_1}}\int P(\tau)\times\exp\left[\frac{i}{2\Phi_0}(\tau-\tau_0)^2+\frac{i}{2\Phi_1}(\tau_1-\tau)^2\right]d\tau, \tag{17}$$

$$h_2(\tau_2,\tau_0)=\frac{1}{2\pi i\sqrt{\Phi_f\Phi_0}}\exp\left(i\frac{\Phi_f-\Phi_2}{2\Phi_f^2}\tau_2^2\right)\times\int\exp\left[\frac{i}{2\Phi_0}(\tau-\tau_0)^2-\frac{i\tau\tau_2}{\Phi_f}\right]P(\tau)d\tau, \tag{18}$$

where Φ_0, Φ_1, and Φ_2 are the GDD parameters of the dispersive medium between the source and the temporal object, between the temporal object and D_1, and between the temporal object and the temporal lens, respectively. In addition, Φ_f characterizes the focal time of the temporal lens, which can be regarded as the effective GDD parameter of the temporal lens, and the GDD parameter of the dispersive medium between the temporal lens and D_2 is also equal to Φ_f. Let $E_1(\tau_1)$ and $E_2(\tau_2)$ be the fields at D_1 and D_2, respectively. Substituting Eqs. (17) and (18) into Eq. (9), we can obtain, according to Eq. (16), the first-order correlation function between these two fields, which is written as

$$\langle E_1^*(\tau_1)E_2(\tau_2)\rangle=\frac{I_0}{4\pi^2\Phi_0\sqrt{\Phi_1\Phi_f}}\exp\left(i\tau_2^2\frac{\Phi_f-\Phi_2}{2\Phi_f^2}\right)\times\int\exp\left[-\frac{i}{2\Phi_1}(\tau_1-\tau)^2-\frac{i\tau\tau_2}{\Phi_f}\right]|P(\tau)|^2d\tau. \tag{19}$$

In scheme I, D_1 is a fast time-resolving detector. In the space domain, a lens and a point detector located at the focus point of the lens form a coherent detection system [31]. Correspondingly, the whole of the temporal lens, D_2, and the dispersive medium between them act as a coherent detection system in the time domain. Thus D_2 should be a fast detector or a point detector in the time domain. The response time of D_2 is shorter than the width of the pulse. Here we let $\tau_2=0$. For simplicity, in this paper we assume the temporal structure function of the temporal object to be real with only two values, zero and 1, so that $|P(\tau)|^2=P(\tau)$. It is noted that the GDD parameter Φ_0 has no impact on the field correlation $\langle E_1^*(\tau_1)E_2(\tau_2)\rangle$ since Φ_0 contributes an equal phase change to the optical field $E_1(\tau_1)$ and $E_2(\tau_2)$. Thus Eq. (19) reduces to

$$\langle E_1^*(\tau_1)E_2(0)\rangle\propto\int\exp\left[-\frac{i}{2\Phi_1}(\tau_1-\tau)^2\right]P(\tau)d\tau, \tag{20}$$

which characterizes the dispersion of the temporal object in the dispersive media similar to the near-field diffraction of an object in the space domain. According to Gaussian moment theorem, the intensity fluctuation correlation can be expressed as

$$\langle\Delta I_1(\tau_1)\Delta I_2(0)\rangle=|\langle E_1^*(\tau_1)E_2(0)\rangle|^2\propto\left|\int\exp\left[-\frac{i}{2\Phi_1}(\tau_1-\tau)^2\right]P(\tau)d\tau\right|^2. \tag{21}$$

Specially, we assume the temporal object to be a temporal grating. The temporal grating is a cycle square pulse sequence which can be constructed by a continuous-wave light source passing through an electro-optic pulse generator. Therefore, the temporal structure function of the temporal grating can be written in the Fourier series

$$P(\tau)=\sum_{n=-\infty}^{\infty}C_n\exp\left(\frac{i2\pi n\tau}{T}\right), \tag{22}$$

where $C_n=\frac{\sin(na\pi)}{n\pi}$, n is an integer, and T and a are the period and duty cycle of the temporal grating, respectively. Substituting Eq. (22) into Eq. (21), we obtain

$$\langle\Delta I_1(\tau_1)\Delta I_2(0)\rangle\propto\left|\sum_n C_n\exp\left(i\pi\frac{n^2}{T^2}2\pi\Phi_1\right)\exp\left(i2\pi\frac{n}{T}\tau_1\right)\right|^2. \tag{23}$$

On the condition that

$$\Phi_1=q\frac{T^2}{\pi}=q\Phi_T, \tag{24}$$

where q is an integer number and $\Phi_T=T^2/\pi$ is defined as the Talbot GDD parameter similar to the Talbot length in the space domain, Eq. (23) thus reduces to

$$\langle\Delta I_1(\tau_1)\Delta I_2(0)\rangle\propto|P(\tau_1)|^2. \tag{25}$$

From the above equation, we can find that the temporal Talbot self-imaging can be achieved through intensity fluctuation correlation measurement.

Furthermore, Eq. (23) can also characterize the fractional Talbot effect. We define

$$a_n=\exp\left(i\pi\frac{n^2}{T^2}2\pi\Phi_1\right), \tag{26}$$

$$g(\tau_1)=\left|\sum_n C_n\exp\left(i\pi\frac{n^2}{T^2}2\pi\Phi_1\right)\exp\left(i2\pi\frac{n}{T}\tau_1\right)\right|^2. \tag{27}$$

If q in Eq. (24) is a fraction number, we write Eq. (24) as

$$\Phi_1=\frac{r}{p}\Phi_T, \tag{28}$$

where r and p are coprime integers. Substituting Eq. (28) into Eq. (26), we have

$$a_n=\exp\left(i2\pi n^2\frac{r}{p}\right), \tag{29}$$

$$a_{n+p}=\exp\left[i2\pi(n+p)^2\frac{r}{p}\right]=\exp\left(i2\pi n^2\frac{r}{p}\right)=a_n. \tag{30}$$

Due to the periodicity of a_n, we can expand a_n in discrete Fourier series as

$$a_n = \frac{1}{p}\sum_{m=0}^{p-1} A_m \exp\left(i2\pi n\frac{m}{p}\right), \tag{31}$$

where the discrete Fourier coefficient A_m satisfies

$$A_m = \sum_{l=0}^{p-1} \exp\left(i2\pi l^2\frac{r}{p}\right)\exp\left(-i2\pi l\frac{m}{p}\right). \tag{32}$$

In terms of the above equation, we get

$$\begin{aligned} g(\tau_1) &= \left|\sum_n C_n a_n \exp\left(i2\pi\frac{n}{T}\tau_1\right)\right|^2 \\ &= \left|\sum_n C_n \frac{1}{p}\sum_{m=0}^{p-1} A_m \exp\left(i2\pi n\frac{m}{p}\right)\exp\left(i2\pi\frac{n}{T}\tau_1\right)\right|^2 \\ &= \left|\frac{1}{p}\sum_{m=0}^{p-1} A_m \sum_n C_n \exp\left[i2\pi n\left(\tau_1+\frac{m}{p}T\right)\Big/T\right]\right|^2. \end{aligned}$$

Combining Eq. (22), we obtain

$$g(\tau_1) = \left|\frac{1}{p}\sum_{m=0}^{p-1} A_m P\left(\tau_1+\frac{m}{p}T\right)\right|^2. \tag{33}$$

It shows that the intensity fluctuation correlation $\langle\Delta I_1(\tau_1)\Delta I_2(0)\rangle$, which is proportional to $g(\tau_1)$, can be expressed as a superposition of finite copies of the original temporal gratings $P(\tau)$ shifted by multiples of $\frac{T}{p}$ and properly modulated. Moreover, we can prove that, for $p=2$, the fractional Talbot image indicated by $g(\tau_1)$ is reproduced exactly but is shifted by half-period $T/2$. For $\Phi_1 = \frac{1}{4}\Phi_T$, the period of the Talbot image is $T/2$. However, for $p=3$, $r=1$, according to Eqs. (32) and (33) and the periodicity of temporal grating, we can obtain

$$\begin{aligned} g(\tau_1) = \frac{1}{3}\Bigg[&|P(\tau_1)|^2 + \left|P\left(\tau_1+\frac{T}{3}\right)\right|^2 + \left|P\left(\tau_1+\frac{2T}{3}\right)\right|^2 \\ &+ 2P\left(\tau_1+\frac{T}{3}\right)P\left(\tau_1+\frac{2T}{3}\right) \\ &- P(\tau_1)P\left(\tau_1+\frac{T}{3}\right) - P(\tau_1)P\left(\tau_1+\frac{2T}{3}\right)\Bigg] \\ \neq\ & g\left(\tau_1+\frac{T}{3}\right) \neq g\left(\tau_1+\frac{2T}{3}\right), \end{aligned} \tag{34}$$

and thus the period of Talbot image isn't $\frac{T}{3}$ or $\frac{2T}{3}$ for this case. Furthermore, for $p=6, 8$, in the same way we prove that the fractional Talbot image hasn't a definite fractional period, which contradicts the results of some articles [9,32].

Accordingly, we plot in Fig. 4 the second-order temporal Talbot carpet, given by the evolution of intensity fluctuation correlation with the GDD parameter Φ_1. To be specific, the period and duty cycle of temporal grating for both Fig. 4 and the following figures are $T = 20$ ps, $a = 0.15$, and $-100 \leqslant n \leqslant 100$, respectively. Hence the Talbot GDD parameter is $\Phi_T = 127$ ps^2. From Fig. 4, we can see that the reproduced imaging of temporal grating can be reconstructed when the

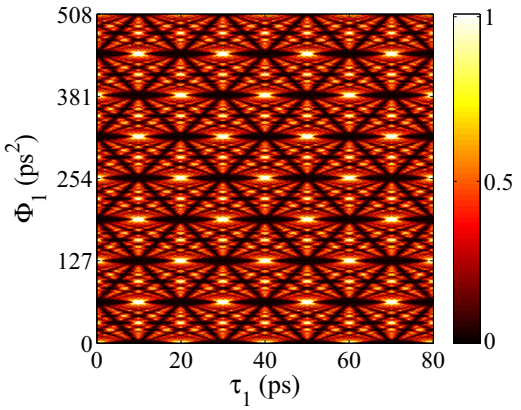

FIG. 4. Temporal Talbot carpet for scheme I, given by the intensity fluctuation correlation with the GDD parameter Φ_1 and the time τ_1.

self-imaging condition $\Phi_1 = q\Phi_T$ is satisfied. However, for $\Phi_1 = \Phi_T/2$, we can also find that the Talbot image is reproduced exactly but is shifted by $T/2$. For $\Phi_1 = \frac{1}{4}\Phi_T$, the period of the Talbot image shown in Fig. 4 is $T/2$. These results coincide with our theoretical analysis.

Next we will discuss scheme II as shown in Fig. 3(b) for second-order temporal Talbot self-imaging effect. The difference between scheme II and scheme I is that no temporal lens exists in scheme II. Following the same way as used in scheme I, the first-order correlation function between the two light fields at the detection plane in scheme II can be expressed in the form

$$\begin{aligned} &\langle E_1^*(\tau_1)E_2(\tau_2)\rangle \\ &= \frac{I_0}{4\pi^2\Phi_0\sqrt{\Phi_1\Phi_2}}\exp\left[\frac{i(\tau_1-\tau_2)^2}{2(\Phi_2-\Phi_1)}\right] \\ &\quad\times\int P(\tau)\exp\left[\frac{i}{2\Phi_{\text{eff}}}\left(\tau-\frac{\Phi_1\tau_2-\Phi_2\tau_1}{\Phi_1-\Phi_2}\right)^2\right]d\tau, \end{aligned} \tag{35}$$

where $\Phi_{\text{eff}} = \frac{\Phi_1\Phi_2}{\Phi_1-\Phi_2}$ denotes the effective GDD parameter. Letting $\tau_2 = 0$, we can express the intensity fluctuation correlation as

$$\begin{aligned} &\langle\Delta I_1(\tau_1)\Delta I_2(0)\rangle \\ &\propto \left|\int P(\tau)\exp\left[\frac{i}{2\Phi_{\text{eff}}}\left(\tau-\frac{\Phi_2\tau_1}{\Phi_2-\Phi_1}\right)^2\right]d\tau\right|^2. \end{aligned} \tag{36}$$

In terms of the self-imaging condition $\Phi_{\text{eff}} = \frac{\Phi_1\Phi_2}{\Phi_1-\Phi_2} = q\Phi_T$ and Eq. (36), the self-imaging for the temporal grating can be achieved as $P(\frac{\Phi_2\tau_1}{\Phi_2-\Phi_1})$. Consequently, the temporal object is changed by a factor $|\frac{\Phi_1}{\Phi_{\text{eff}}}| = |1-\frac{\Phi_1}{\Phi_2}|$, that is to say, the image of the temporal grating can be enlarged or shrunk. Moreover, the effective GDD parameter for self-imaging can be adjusted not only by the parameter in path 1 but also by path 2 since $\Phi_1 = \frac{q\Phi_T\Phi_2}{q\Phi_T-\Phi_2}$.

According to Eq. (36) and assuming the GDD parameter $\Phi_1 = 254$ ps^2, we plot the temporal Talbot carpet in Fig. 5, that is, the evolution of intensity fluctuation correlation as a function of the effective GDD parameter Φ_{eff}. From Fig. 5,

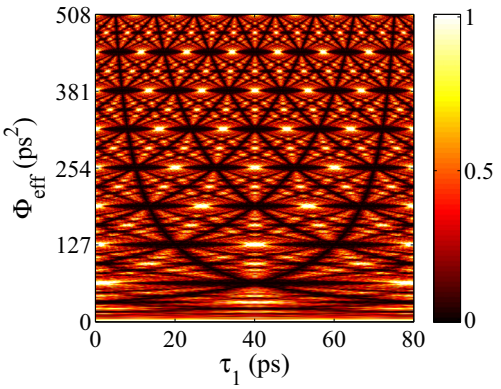

FIG. 5. Temporal Talbot carpet for scheme II, given by the intensity fluctuation correlation with the effective GDD parameter Φ_{eff} and the time τ_1.

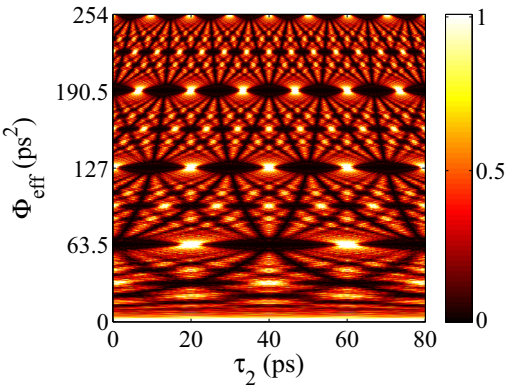

FIG. 6. Temporal Talbot carpet for scheme III, given by the intensity fluctuation correlation with the effective GDD parameter Φ_{eff} and the time τ_2.

we can see that, when $\Phi_{\text{eff}} = 127$ ps^2, the image is enlarged with a period of 40 ps, yet when $\Phi_{\text{eff}} = 508$ ps^2, the image is shrunk with a period of 10 ps. Furthermore, we can see, when Φ_{eff} is equal to Φ_1, the temporal grating is reproduced.

Finally we analyze the second-order temporal Talbot effect with scheme III as shown in Fig. 3(c). The temporal object is placed in path 1 after the fiber beam splitter similar to the temporal ghost imaging. In the same way, the first-order correlation function can be expressed in the form

$$\langle E_1^*(\tau_1)E_2(\tau_2)\rangle = \frac{I_0}{2\pi\sqrt{\Phi_1(\Phi_2-\Phi_0)}}\exp\left[\frac{i(\tau_1-\tau_2)^2}{2(\Phi_2-\Phi_1-\Phi_0)}\right] \times \int \exp\left\{\frac{i}{2\Phi_{\text{eff}}}\left[\tau+\frac{\tau_1(\Phi_2-\Phi_0)-\tau_2\Phi_1}{\Phi_1-\Phi_2+\Phi_0}\right]^2\right\}P(\tau)d\tau, \tag{37}$$

where Φ_0, Φ_1, and Φ_2 are the GDD parameters of the dispersive medium between the source and the temporal object, between the temporal object and D_1, and between the source and D_2, respectively. In addition, the effective GDD parameter is defined as $\Phi_{\text{eff}} = \frac{\Phi_1(\Phi_2-\Phi_0)}{\Phi_1-(\Phi_2-\Phi_0)}$. The intensity fluctuation correlation then can be written as

$$\langle \Delta I_1(\tau_1)\Delta I_2(\tau_2)\rangle \propto \left|\int \exp\left\{\frac{i}{2\Phi_{\text{eff}}}\left[\tau-\frac{\tau_2\Phi_1-\tau_1(\Phi_2-\Phi_0)}{\Phi_1-\Phi_2+\Phi_0}\right]^2\right\}P(\tau)d\tau\right|^2. \tag{38}$$

The above equations imply that the second-order temporal Talbot self-imaging effect can be considered as the consequence of the joint dispersion, which plays the same role as that of the joint diffraction in second-order spatial Talbot effect, between the correlated fields.

From Eq. (38), one can see that the image of the temporal grating now can be obtained as $P(\frac{\tau_2\Phi_1-\tau_1(\Phi_2-\Phi_0)}{\Phi_1-\Phi_2+\Phi_0})$. For scheme III, the image of temporal grating can be enlarged or shrunk if D_1 or D_2 is a point detector in the time domain. Here let $\tau_1 = 0$ and $\Phi_1 = 127$ ps^2. Accordingly, the temporal Talbot carpet for scheme III is plotted in Fig. 6 in terms of Eq. (38), where we can also see that the image of temporal grating can be recovered, enlarged, or shrunk. This result implies that the Talbot effect based on intensity fluctuation correlation could be useful to multiply the repetition rate of the temporal signal [33]. As for special case $\Phi_2 = \Phi_0$, the image of the temporal object with period unchanged can be reconstructed. For this case scheme III resembles the temporal ghost imaging scheme where the temporal object can be nonperiodic. In addition, if the path 2 is removed, a computational correlated Talbot self-imaging scheme can be constructed. In this computational correlated Talbot self-imaging scheme, a point detector in the time domain can be used to detect a fast periodic pulse signal.

Remark. Due to the fact that the temporal Talbot effect is a near-field dispersion effect, the quadratic phase factor $\tau^2/(2\Phi_1)$ in Eq. (21) can't be neglected for the scheme I. In terms of the near-field dispersion condition and our theoretical analysis, in the experimental application, for a temporal grating with a limited length $\tau_{\max}$, it is appropriate that $\Phi_T/4 < \Phi_1 < \tau_{\max}^2/2$. To be specific, we assume the dispersive media are standard silica fibers. The group-velocity dispersion coefficient $\beta \sim 50$ ps^2/km in the visible light region [34]. Accordingly, for a temporal grating with the length $\tau_{\max} \sim 10^2$ ps and the period $T = 25$ ps, the experimental scale of the propagation distance l_1, between the source and the detector D_1, is 1 km $< l_1 = \Phi_1/\beta < 100$ km. In addition, the response time of the detectors, which is shorter than the pulse width of the temporal grating, is of the magnitude of picosecond in favor of experimental observation. For schemes II and III, the corresponding experimental scales can also be taken in the same way.

IV. CONCLUSION

In conclusion, we have investigated the second-order Talbot self-imaging effect with temporally incoherent light. The results have shown that the self-imaging of a periodic signal can be extracted through the intensity fluctuation correlation measurement. In view of space-time duality, this second-order temporal Talbot self-imaging effect can be considered as the consequence of the joint dispersion between the correlated fields. Furthermore, one could use a point detector to detect a fast signal based on computational correlated Talbot

effect in the time domain. According to the discrete Fourier transformation, we find the fractional Talbot self-imaging doesn't generally possess a definite fractional period, which contradicts some articles' results.

The temporal pulses traveling in dispersive media usually appear as distortion and interference due to the dispersion. However, based on the Talbot effect via intensity fluctuation correlation, our results could have potential application in transferring a periodic signal in optical fiber or multiplying the repetition frequency of the input light pulse sequence without the requirement of dispersion cancellation or compensation.

ACKNOWLEDGMENTS

This work was supported by the National Natural Science Foundation of China (CN), Project No. 11604243, and the Natural Science Foundation of Tianjin, Project No. 16JCQNJC01600.

[1] H. F. Talbot, Philos. Mag. **9**, 401 (1836).
[2] L. Rayleigh, Philos. Mag. **11**, 196 (1881).
[3] P. Xi, C. Zhou, E. Dai, and L. Liu, Opt. Express **10**, 1099 (2002).
[4] R. Iwanow, D. A. May-Arrioja, D. N. Christodoulides, G. I. Stegeman, Y. Min, and W. Sohler, Phys. Rev. Lett. **95**, 053902 (2005).
[5] F. Pfeiffer, M. Bech, O. Bunk, P. Kraft, E. F. Eikenberry, C. Brönnimann, C. Grünzweig, and C. David, Nat. Mater. **7**, 134 (2008).
[6] K.-H. Luo, J.-M. Wen, X.-H. Chen, Q. Liu, M. Xiao, and L.-A. Wu, Phys. Rev. A **80**, 043820 (2009).
[7] C. H. R. Ooi and B. L. Lan, Phys. Rev. A **81**, 063832 (2010).
[8] X.-B. Song, H.-B. Wang, J. Xiong, K. Wang, X. Zhang, K.-H. Luo, and L.-A. Wu, Phys. Rev. Lett. **107**, 033902 (2011).
[9] K.-H. Luo, X.-H. Chen, Q. Liu, and L.-A. Wu, Phys. Rev. A **82**, 033803 (2010).
[10] X.-B. Song, J. Xiong, X. Zhang, and K. Wang, Phys. Rev. A **82**, 033823 (2010).
[11] J. Wen, Y. Zhang, and M. Xiao, Adv. Opt. Photon. **5**, 83 (2013).
[12] R. Salem, M. A. Foster, and A. L. Gaeta, Adv. Opt. Photon. **5**, 274 (2013).
[13] M. A. Foster, R. Salem, D. F. Geraghty, A. C. Turner-Foster, M. Lipson, and A. L. Gaeta, Nature (London) **456**, 81 (2008).
[14] J. Schröder, F. Wang, A. Clarke, E. Ryckeboer, M. Pelusi, M. A. Roelens, and B. J. Eggleton, Opt. Commun. **283**, 2611 (2010).
[15] B. H. Kolner, IEEE J. Quantum Electron. **30**, 1951 (1994).
[16] M. Fridman, A. Farsi, Y. Okawachi, and A. L. Gaeta, Nature (London) **481**, 62 (2012).
[17] T. Shirai, T. Setälä, and A. T. Friberg, J. Opt. Soc. Am. B **27**, 2549 (2010).
[18] T. Setälä, T. Shirai, and A. T. Friberg, Phys. Rev. A **82**, 043813 (2010).
[19] Z. Chen, H. Li, Y. Li, J. Shi, and G. Zeng, Opt. Eng. **52**, 076103 (2013).
[20] P. Ryczkowski, M. Barbier, A. T. Friberg, J. M. Dudley, and G. Genty, Nat. Photonics **10**, 167 (2016).
[21] F. Devaux, P.-A. Moreau, S. Denis, and E. Lantz, Optica **3**, 698 (2016).
[22] F. Devaux, K. P. Huy, S. Denis, E. Lantz, and P.-A. Moreau, J. Opt. **19**, 024001 (2016).
[23] P. Ryczkowski, M. Barbier, A. T. Friberg, J. M. Dudley, and G. Genty, APL Photon. **2**, 046102 (2017).
[24] Y. O-oka and S. Fukatsu, Appl. Phys. Lett. **111**, 061106 (2017).
[25] X. Yao, W. Zhang, H. Li, L. You, Z. Wang, and Y. Huang, Opt. Lett. **43**, 759 (2018).
[26] J. Liu, J. Wang, H. Chen, H. Zheng, Y. Liu, Y. Zhou, F.-L. Li, and Z. Xu, Opt. Commun. **410**, 824 (2018).
[27] Y. K. Xu, S. H. Sun, W. T. Liu, G. Z. Tang, J. Y. Liu, and P. X. Chen, Opt. Express **26**, 99 (2018).
[28] J. W. Goodman, *Introduction to Fourier Optics* (McGraw-Hill, New York, 1968).
[29] H. A. Haus, *Waves and Fields in Optoelectronics* (Prentice-Hall, Englewood Cliffs, NJ, 1984).
[30] S. Hartmann and W. Elsäßer, Sci. Rep. **7**, 41866 (2017).
[31] X.-B. Song, D.-Q. Xu, H.-B. Wang, J. Xiong, X. Zhang, D.-Z. Cao, and K. Wang, Appl. Phys. Lett. **103**, 131111 (2013).
[32] V. Torres-Company, J. Lancis, H. Lajunen, and A. T. Friberg, Phys. Rev. A **84**, 033830 (2011).
[33] J. Azaña and M. A. Muriel, Opt. Lett. **24**, 1672 (1999).
[34] G. P. Agrawal, *Nonlinear Fiber Optics* (Academic Press, Oxford, 2013).